AD-A162 472 CHARACTERIZATION OF A CHARGE INJECTION DEVICE CAMERA SYSTEM FOR SPECTROCH (U) ARIZONA UNIV TUCSON DEPT OF CHEMISTRY G R SIMS ET AL 25 NOV 85 TR-40 1/1

UNCLASSIFIED N00014-83-K-0268 F/G 14/5 NL

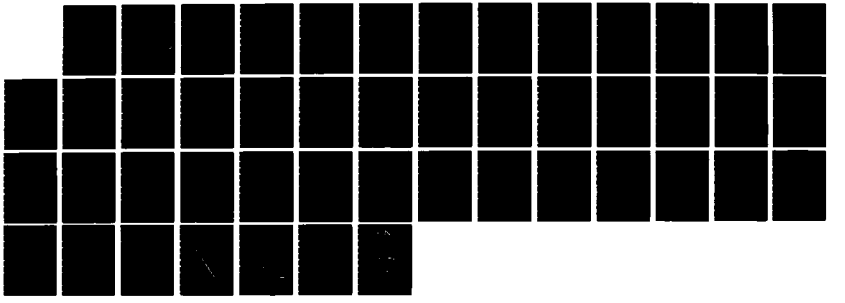

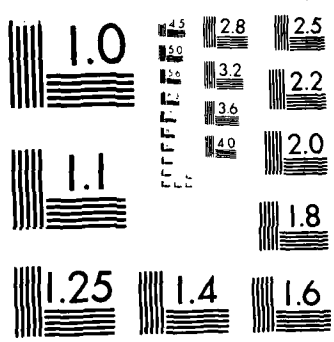

MICROCOPY RESOLUTION TEST CHART
NATIONAL BUREAU OF STANDARDS 1963-A

SECURITY CLASSIFICATION OF THIS PAGE (When Data Entered)

REPORT DOCUMENTATION PAGE

READ INSTRUCTIONS BEFORE COMPLETING FORM

1. REPORT NUMBER: 40	2. GOVT ACCESSION NO.
3. RECIPIENT'S CATALOG NUMBER	
4. TITLE (and Subtitle): Characterization of a Charge Injection Device Camera System for Spectrochemical Measurements	5. TYPE OF REPORT & PERIOD COVERED: Interim
6. PERFORMING ORG. REPORT NUMBER	
7. AUTHOR(s): G.R. Sims and M.B. Denton	8. CONTRACT OR GRANT NUMBER(s): N00014-83-K-0263
9. PERFORMING ORGANIZATION NAME AND ADDRESS: Department of Chemistry, University of Arizona, Tucson, Arizona 85721	10. PROGRAM ELEMENT, PROJECT, TASK AREA & WORK UNIT NUMBERS: NR 051-549
11. CONTROLLING OFFICE NAME AND ADDRESS: Office of Naval Research, Arlington, Virginia 22217	12. REPORT DATE: November 25, 1985
	13. NUMBER OF PAGES: 45
14. MONITORING AGENCY NAME & ADDRESS(if different from Controlling Office)	15. SECURITY CLASS. (of this report): Unclassified
	15a. DECLASSIFICATION/ DOWNGRADING SCHEDULE

AD-A162 472

16. DISTRIBUTION STATEMENT (of this Report)

[illegible] is unlimited.

17. DISTRIBUTION STATEMENT (of the abstract entered in Block 20, if different from Report)

DTIC ELECTE DEC 18 1985 D

18. SUPPLEMENTARY NOTES

Prepared for publication in Journal of Applied Optics

19. KEY WORDS (Continue on reverse side if necessary and identify by block number)

Charge Injection Device (CID)

20. ABSTRACT (Continue on reverse side if necessary and identify by block number)

An electronic camera system employing a General Electric Co. CID-111 Charge Injection Device (CID) detector is described. Unique capabilities of this camera system, including destructive and nondestructive readout modes, signal-to-noise enhancement through multiple nondestructive readouts, and pseudo random pixel addressing are discussed. The performance characteristics related to spectrometric applications are presented. Parameters discussed include sensitivity, linearity, noise, dynamic range, blooming, pixel crosstalk, and spectral response.

DD FORM 1 JAN 73 1473 EDITION OF 1 NOV 65 IS OBSOLETE

S/N 0102-LF-014-6601

SECURITY CLASSIFICATION OF THIS PAGE (When Data Entered)

FILE COPY

OFFICE OF NAVAL RESEARCH

Contract N00014-83-K-0268

Task No. 051-549

TECHNICAL REPORT NO. 40

Characterization of a Charge Injection Device Camera System for Spectrochemical Measurements

by

G.R. Sims and M.B. Denton

Prepared for publication in the

Journal of Applied Optics

University of Arizona
Department of Chemistry
Tucson, Arizona 85721

DTIC
ELECTE
DEC 18 1985
D

November 25, 1985

Reproduction in whole or in part is permitted for any purpose of the United States Government

DISTRIBUTION STATEMENT A
Approved for public release;
Distribution Unlimited

85 12 [illegible] 05

CHARACTERIZATION OF A CHARGE INJECTION DEVICE CAMERA SYSTEM AS A SPECTROSCOPIC DETECTOR

G. R. Sims and M. B. Denton
University of Arizona
Tucson, AZ 85721

ABSTRACT

An electronic camera system employing a General Electric Co. CID-11B charge injection device (CID) detector is described. Unique capabilities of this camera system, including destructive and non-destructive readout modes, signal to noise enhancement through multiple non-destructive readouts, and pseudo random pixel addressing are discussed. The performace characteristics related to spectrometric applications are presented. Parameters discussed include sensitivity, linearity, noise, dynamic range, blooming, dark current, pixel crosstalk, and spectral response.

Accession For
NTIS GRA&I
Codes
or
Special
A1

INTRODUCTION

Optical spectrometry is widely employed as an analytical tool in nearly every scientific discipline. Spectrometric techniques that utilize the principles of emission, fluorescence, and absorption, are routinely used to probe the chemical and physical nature of an ever increasing range of materials for science, engineering, and industry. The popularity of analytical spectrometry is in part due to the wealth of information about a sample available from a spectroscopic probe. In order to take full advantage of this information, the spectrometric system must quickly and accurately measure the spectral signal from a sample, preferably at all wavelengths simultaneously. The nature of this signal is typically a wide dynamic range photon flux that covers a broad wavelength range. The present generation of instrumentation for the UV-VIS spectral region is incapable of taking full advantage of this spectral information, and this has been a motivating force behind a research effort aimed at improving spectroscopic instrumentation that has spanned many years.

The state of the art spectrometer for analytical UV-VIS applications is a dispersion monochomator or polychromator utilizing photomultiplier tube(s) and/or photographic emulsions as detectors. A high resolution polychromator is a choice method of separating spectral information into its components, but the detectors employed severely limit the overall performance of the system. Photomultiplier tube detectors cannot cover the number of desired channels within a reasonable timeframe and photographic film is far too inaccurate and too time consuming to develop and read. Interferometric techniques such as those so successfully used in the infrared spectral region have not been found to be generally useful in the UV-VIS because of

the increased complexity and cost of instrumentation and unacceptably high noise levels imposed on weak spectral features due to the photon shot noise from intense features (1). This has caused investigations to focus on finding a suitable parallel multichannel detector system to replace photomultiplier tubes and photographic emulsions for dispersion spectrometers.

For many years, interest has been focused towards using one of a variety of optoelectronic imaging detector (OID) or "TV type" detector for this application. A variety of OIDs, both tube type and solid state, has been investigated for potential use in optical spectrometry, but none has been found to be completely suitable for one of a number of reasons. In order to be generally suitable for most spectroscopic applications, an OID must meet the following requirements;

(a) good quantum efficiency over a wide spectral range,

(b) low readout noise,

(c) wide dynamic range,

(d) electronic readout,

(e) large number of resolution elements,

(f) no crosstalk or blooming among individual detectors,

(g) free of readout lag, and

(h) economically feasible to acquire and operate.

Tube type OIDs, such as the vidicons, orthocon, isocon, and image dissector, have all been examined by a number of investigators, but none has been found to be entirely suitable (2,3,4). That is not to say that some of these devices are not very useful and appropriate for some specific spectroscopic applications, but these devices are not acceptable as general optical spectrometric detectors.

THE SILICON PHOTODIODE ARRAY

In the past few years, a variety of silicon optical array detectors built with integrated circuit photofabrication technology has been produced and a few of these devices have been investigated as to their potential as general purpose spectroscopic detectors. Because of the stringent requirements put on a detector for this application, only the self scanning silicon photodiode array (PDA) has found some acceptance at this time. The limited success that the PDA has experienced is partially due to manufacturers of PDAs making devices specifically for spectroscopic applications. For example, the EG+G Reticon "S" series PDA.

The "S" series PDA has many attributes that make it a potentially attractive detector for a many spectroscopic applications. Among these are:

(a) high quantum yield in the near IR, visible, and ultraviolet regions;

(b) moderately high dynamic range, about 10,000:1;

(c) high degree of geometrical accuracy; and

(d) ready availability and easy implementation in a camera system.

In addition, this device has a relatively large size of 25 microns by 2.5 millimeters for each detector (also known in OID nomenclature as a picture element or PIXEL). This gives the device a high charge capacity, and thus increases the dynamic range. Also, the 100:1 height-to-width aspect ratio of the pixels is seen as an advantage when coupling this device to a conventional polychromator designed for photographic detection.

The PDA also has several shortcomings which have limited its success. Among these are:

(a) very high noise level compared to photomultiplier tubes;

(b) availability with a very limited number of pixels;

(c) susceptibility to blooming; and

(d) high cost

Several articles in the literature describe the fundamentals and operating characteristics of PDAs (5,6). Based on the design and readout mechanism of the PDA, it can be concluded that the high readout noise of the PDA is an inherent characteristic of the device and can not be significantly reduced without greatly compromising the dynamic range of the device. Although all PDAs are susceptible to blooming, this is generally not a major problem with the "S" series devices due to their high charge capacity. One of the major shortcomings of PDAs is the low number of resolution elements. The Reticon "S" series device is currently available in a maximum of 1024 pixels. This is inadequate to simultaneously cover the UV and visibile spectral regions with adequate resolution for even the least demanding applications. Other types of PDAs with more pixels are available, including a 4096 element linear array and a two dimensional array with 65,384 pixels arranged in a 256X256 element format, but these devices are much less suitable for spectroscopic applications because of higher noise levels and much lower dynamic range.

THE CHARGE COUPLED DEVICE

Another silicon array detector that has received some interest in the literature is the Charge Coupled Device (CCD). This device holds much promise for some types of analytical spectroscopic techniques, but present devices are not suitable for universal application. By virtue of its readout mechanism and small pixel area, the CCD typically has very low readout noise, low charge capacity and a high susceptibility to blooming. Most commercially available CCDs have limited blue and no ultraviolet

response, although some devices that respond very well throughout the visible and ultraviolet are now becoming available. Devices which feature blooming control have also been introduced (7,8), but these have not yet been evaluated for spectroscopic applications. In general, the current generation of CCD is capable of being an excellent low light level detector, but its use is restricted to applications that have limited dynamic range and no intense spectral features. CCD arrays are commercially available with a large number of resolution elements such as linear devices of over 4000 pixels and area devices of over 4,000,000 pixels (7).

THE CHARGE INJECTION DEVICE

The Charge Injection Device (CID) has been commercially available from the General Electric Co. since 1974. A CID is a two dimensonal array of optical detectors built with metal-oxide-semiconductor type integrated circuit technology. A single pixel site of the CID consists of two polysilicon electrodes separated from a N doped silicon epitaxial layer with thin silicon dioxide insulation. The electrodes are biased such that they form an inversion region in the epitaxial layer where photon generated charge is collected. By controlling the bias on the electrodes, charge can be made to transfer between the two electrodes, which provides a means of measuring the charge in a pixel site. Charge can be cleared from a pixel by removing the bias from both electrodes simultaneously. References 10 through 15 give a description of the structure of a CID and typical readout modes.

Because the readout process in a CID involves a reversible intracell charge transfer, it is possible to re-read the charge in a pixel as many times a desired (12,14,15). This readout mode is termed non-destructive

readout (NDRO) and is a unique characteristic of the CID. By averaging many successive NDROs, the temporal read noise of a CID imaging system can be greatly diminished (16). Although spectroscopic concerns did not dictate the design of the CID, many features of the device make it an attractive candidate as a scientific imaging detector. For instance, the sample charge transfer scheme used in the CID makes the device inherently resistant to blooming (12). Also, the simple electrode structure leaves much silicon exposed to incident radiation which in turn leads to high quantum efficiency. Finally, the simple x,y pixel addressing scheme permits random or pseudo-random pixel addressing (10,15).

THE UA/CID-11B IMAGING SPECTROSCOPIC DETECTOR SYSTEM

The CID-11B sensor was designed for use in a RS170 robotics/surveillance video camera. This camera (General Electric model TN2200) does not support many capabilities of the CID-11, namely non-destructive readout, pseudo random pixel access, ultraviolet radiation sensitivity, and low noise operation. For this reason, a totally new imaging detector system based on the CID-11B sensor has been designed and constructed at the University of Arizona for use in spectroscopic studies. This system, which has been previously described (17) consists of a cryogenically cooled sensor head, a high speed digital imager controller, and a host computer system. Cooling the CID sensor is necessary to reduce the thermal generation of charge. The UA/CID-11B sensor head employs liquid nitrogen to cool the sensor to approximately 77 K. At this temperature, no thermal charge can be detected after several hours of integration.

The sophisticated and flexible design of the UA/CID-11B system has allowed the determination of many characteristics of the device which have

been previously unknown. This crucial information permits an accurate comparison of the CID to other multichannel spectroscopic detectors.

UNIVERSAL TEST CHAMBER

Many of the characterizaton studies subsequently described were conducted in an environmentally controlled test chamber. The entire sensor head was placed inside this chamber while experiments were being conducted. The temperature in tnis chamber was maintained at 27 ± 0.1°C. This regulation minimized thermal drift in sensitive analog electronic circuits which had previously been recognized as a source of substantial error.

The light emitting diodes (LEDs) were placed in the chamber 30 cm from the sensor head and oriented to provide uniform illumination of the CID. Current to the LEDs was controlled via the imager controller which allowed LED on/off time resolution of 500 nsec.

DETERMINATION OF SYSTEM GAIN

In order to accurately assess the photometric performance of the UA/CID-11B system and to make fair comparisons to similar detector systems, the quantity of charge in a pixel which will produce a given analog to digital converter count (the system gain) must be accurately known. The system gain of any array detector system may be estimated from the electronic components and circuitry used, but such an estimate is likely to be very inaccurate since exact values for specific electronic components used are typically not known.

In order to make an accurate determination of system gain for the UA/CID-11B system, a procedure similar to the mean-variance method described by Fowler and Mortara was developed (18). The mean-variance method is an especially attractive approach to system gain measurements as the necessary apparatus is modest and the experimental procedure is simple to execute.

THE MEAN-VARIANCE METHOD

The principles of the mean-variance method can be illustrated by considering a single pixel of a detector array. Assume that this pixel initially contains no charge, then a number of electron hole separation events occur generating a mean quantity of charge equal to $\bar{q}$ electrons (a charge injection device actually stores positive charge, but the quantity of charge can be expressed in terms of equivalent electrons). When the pixel is read out, the mean signal read by the computer due to the charge in the pixel will be $\bar{S}$ analog to digital converter units (ADUs). Whether the charge is generated from the absorbtion of photons or from thermal excitation, Poisson statistics will be followed. It follows then that shot noise due to charge separation events, $\delta_{(e)}$ is a predictable quantity dependent only on the total amount of charge in the pixel.

$$\delta_{(e)} = (\bar{q})^{1/2} \tag{1}$$

The mean signal is related to the number of electrons in the pixel by the system gain:

$$\bar{S} = G\bar{q} \tag{2}$$

Where G is the gain in ADUs/electron. Likewise, the event shot noise expressed as ADUs, $\delta_{(E)}$ will be:

(3) $$\delta_{(E)} = G\delta_{(e)}$$

By substituting Equation 2 into Equation 3:

(4) $$\delta_{(E)} = G(\bar{q})^{1/2}$$

and squaring equation 4 and substituting $\bar{S}/G$ for $\bar{q}$ (Equation 2):

(5) $$\delta^2_{(E)} = G\bar{S}$$

an equation results which indicates the system gain can be calculated if a signal level and the variance in signal level due to event shot noise are known. Unfortunately, variance from shot noise alone can not be independently determined as it can not be isolated from the electronic noise sources associated with pixel readout (system read noise). It is important to note, however, that system read noise is due to various noise sources in the detector and amplifier which are independent of the quantity of charge in a pixel (system read noise is discussed in a later section). If it is assumed that the read noise is equal to n equivalent electrons, the read noise expressed in ADUs, $\delta_{(N)}$ will be:

(6) $$\delta_{(N)} = Gn$$

Similarly, variance due to system read noise will be:

(7) $$\delta^2_{(N)} = G^2N^2$$

and the net signal variance from all noise sources, $\delta_{(S)}$ will be:

(8) $$\delta^2_{(S)} = G\bar{Q} + G^2N^2$$

This is an equation of the form $Y = mX + b$. If mean signal in ADUs is plotted versus total signal variance in ADUs, a straight line results with a slope of G and intercept of G^2N^2.

MEAN-VARIANCE MEASUREMENTS OF CHARGE INJECTION DEVICES

The CID has several unique characteristics that complicate the determination of system gain by conventional mean-variance method and would lead to systematic errors and inaccurate results if not taken into account. Because of this, a new experimental procedure for mean-variance measurements designed specifically for CID camera systems was developed.

A potentially major source of error in determining the mean signal for a subarray of the CID-11B detector is due to a phenomona known as row-column crosstalk (19). Row-column crosstalk can cause the signal from a pixel to appear erroneously high because the measured signal results from both the charge in that pixel, plus an additional crosstalk signal proportional to a fraction of the sum of all charge in all pixels located on the same row as the pixel being read. If no compensation for row-column crosstalk is made, the calculated system gain from a mean-variance plot will be erroneously low.

ROW-COLUMN CROSSTALK CORRECTION

Row-column crosstalk correction can be accomplished by simply determining and subtracting the crosstalk signal for all pixels located on a given row from the net signal of each pixel on that same row. This is possible only because the row-column crosstalk signal is identical for all pixels located on a common row.

The magnitude of the row-column crosstalk signal for pixels of any row of the array can be determined by measuring the signal from pixels in a region of the row which is not illuminated before and after the remaining pixels of the row are illuminated. The increase in signal for the non-illuminated pixels may be attributed only to row-column crosstalk. In practice, this is accomplished by covering a portion of the CID with an opaque mask and reading signals from pixels under this mask to determine the crosstalk signal.

When it is desired to compute a crosstalk-free mean signal from a subarray of pixels as is the case in mean-variance measurements, an independent crosstalk correction does not need to be performed on every pixel of the subarray. Rather, a mean crosstalk signal can be computed for the entire subarray by using two subarrays which share common rows, one in an illuminated region of the CID and one in a non-illuminated region. By recording the mean signals for each subarray before and after one subarray is illuminated and subtracting the mean increase in signal for the non-illuminated subarray from the mean increase for the illuminated subarray, the illuminated subarray is corrected for row-column crosstalk.

DETERMINATION OF GAIN FOR THE UA/CID-11B SYSTEM

Mean-variance measurements on the UA/CID-11B camera system were conducted in the universal test chamber with the sensor head cooled to operating temperature. To facilitate row-column crosstalk correction, only a 40 by 40 pixel region near the center of the array was illuminated. The remainder of the array was covered with an opaque mask.

Mean-variance measurements were conducted by reading data from two 20 by 20 pixel subarrays in the CID. One subarray was located in the center of the illuminated area and the other located well under the mask. The subarray in the masked area had the same Y axis origin as the subarray in the illuminated area, indicating that both subarrays were located on common rows. Data was collected for a single point in the mean-variance plot by first injecting the entire array of all charge, then reading the subarrays in both the illuminated area and the masked ("dark") area. The means of these two subarrays were then calculated and the results stored. Next, the LED was flashed "X" number of times (X was experimentally established to give an appropriate increase in signal) and both subarrays read again. The means of the two subarrays were again calculated and stored. In addition, the signal from each pixel in both subarrays was stored as this data was used later in calculating signal variance. The entire inject, read, flash X times, and read process was repeated ten times for a single point on the mean-variance plot.

The mean signal due to charge in the pixels in the illuminated subarray was calculated from;

$$(9) \qquad \bar{S}_{(q)} = (\bar{S}_{(l,x)} - \bar{S}_{(l,0)}) - (\bar{S}_{(d,x)} - \bar{S}_{d,0)})$$

where:

$\bar{S}_{(q)}$ = mean signal due to charge in the pixels of the illuminated area

$\bar{S}_{(l,x)}$ = mean signal from illuminated area after X LED flashes

$\bar{S}_{(l,0)}$ = mean signal from pixels in light area before flashes

$\bar{S}_{(d,x)}$ = mean signal from pixels in dark area after X LED flashes

$\bar{S}_{(d,0)}$ = mean signal from pixels in dark area before flashes.

Subtracting the mean signal obtained before the flashes from the mean signal obtained after the flashes cancels any differences in amplifier offset between the two areas. The amplifier is normally set for a positive offset of approximately 200 ADUs, but the exact offset may be different in the two areas due to slight differences in capacitance of the column electrodes of the pixels.

The pixels in the dark area do not collect any charge during the flashes, which means the average signal from the dark subarray is equal to the mean crosstalk signal for the illuminated area. The $\bar{S}_{(q)}$ values calculated for each of the ten trials are averaged to give the value used as the mean for one point on the mean-variance plot.

The variance for each point of the mean-variance plot is calculated by first subtracting the mean signal of the illuminated and dark subarrays from the signal from each pixel in the respective subarray:

$$S'_{(i,l)} = S_{(i,l,x)} - \bar{S}_{(l,x)} \tag{10}$$

and

$$S'_{(i,d)} = S_{(i,d,x)} - \bar{S}_{(d,x)} \tag{11}$$

where:

$S_{(i,l,x)}$ = signal from pixel "i" in the illuminated area after X LED flashes

$S_{(i,d,x)}$ = signal from pixel "i" in the dark area after X LED flashes.

This adjusts the mean of each subarray to zero and thus ensures that any signal variance due to slight changes in the LED flash intensity is cancelled out. Next, the variance for a single pixel is calculated from the data obtained during the ten trials:

$$(12) \qquad \delta^2_{(i,l)} = \frac{1}{9} \sum_{1}^{10} (S'_{(i,l,j)} - \bar{S}'_{(i,l)})^2$$

and

$$(13) \qquad \delta^2_{(i,d)} = \frac{1}{9} \sum_{1}^{10} (S'_{(i,d,j)} - \bar{S}'_{(i,d)})^2$$

where:

$S'_{(i,l,j)}$ = adjusted signal from pixel "i", trial "j" in the illuminated area

$S'_{(i,d,j)}$ = adjusted signal from pixel "i", trail "j" in the dark area

$\bar{S}'_{(i,l)}$ = mean of pixel "i" in the illuminated area for all ten trials

$\bar{S}'_{(i,d)}$ = mean of pixel "i" in the dark area for all ten trials.

These individual pixel variances were then averaged for the 400 pixels in each subarray. The average variance for the dark subarray was subtracted from the average variance for the illuminated subarray to yield the variance figure used for the mean-variance plot. Subtracting the variance from the dark subarray removes a slight variance contribution due to row-column crosstalk and the variance due to system read noise.

To collect the points used for the mean-variance plot, the process discussed above was repeated with 2X, 3X, 4X...10X LED flashes. The entire mean-variance experiment was then repeated seven times and the data from the seven experiments averaged. Data for five points that fall within the range where the signal from a pixel is linearly proportional to the quantity of charge in that pixel is plotted in Figure 1. The slope of the best line through these data points was determined with a weighted least-squares fit to be 1.348×10^{-3} ADUs/electron (741.6 electrons/ADU) with a standard deviation of 0.548 ADUs/electron (1.8 electrons/ADU).

SYSTEM READ NOISE AND PATTERN RESPONSE

In spectroscopic applications the noise of a detector system is a major concern because this parameter very often dictates the performance of the system at low light levels. Types of noise in array detectors can be divided into two general categories: one known as temporal (time dependent) read noise and the other historically known as fixed pattern noise. Temporal read noise can be described as the sum of all noise sources (other than charge generation event shot noise) that cause the signal from an individual detector element to vary in time. On the other hand, fixed

pattern noise is due to different response characteristics (specifically signal offsets) of the individual pixels of an array detector and thus are not temporal in nature. Fixed pattern noise is a major concern only in array detector systems where no signal processing is performed. In modern computerized array detector systems, pattern noise can not be considered a real noise source since it can be eliminated by signal subtraction or other simple computational methods. For this reason, the term fixed pattern response will be used throughout this communication as a more accurate description of spatial variations in signal offsets of the CID-11B detector.

SOURCES OF TEMPORAL READ NOISE

The components of temporal read noise for a CID camera system can be divided into two general categories: noise originating in the CID detector itself, and noise associated with the video amplifier and drive circuitry. Predominant sources of noise in CIDs have been attributed to Johnson noise from resistance in the array conductors (principally row and column polysilicon electrodes), and Johnson noise from the channel resistance of the row and column select switches (16). Major sources of noise in a video preamplifier such as the one used in the UA/CID-11B system are typically Johnson noise from the channel resistance of the input FET, shot noise from leakage currents in the input FET, and 1/f noise (20). Voltage spikes and ripple on clock lines of the row and column shift registers and the vertical enable line may couple into the video line to some degree adding yet another potential noise source. On the other hand, switch noise (or kTC noise) is not a major noise source in a CID camera system such as the one built for this study because of the double correlated sampling used in the readout scheme (19,21).

MEASUREMENT OF TEMPORAL READ NOISE

The unique non-destructive readout capability of the CID allows a simple, yet accurate method of measuring temporal noise for the UA/CID-11B system. The principle behind this method is illustrated by considering a single pixel within the CID array. Assume this pixel initially contains no charge, then a number of charge separation events occur, creating an average of $\bar{q}$ electrons in the pixel. There is an event shot noise associated with the creation of this charge which means the exact quantity of charge in the pixel can not be predicted. It is important to note, however, that the number of electrons created in the pixel is an exact, fixed quantity despite the event shot noise.

Once charge generation is stopped, the system read noise may be determined by simply making two non-destructive reads of the pixel and subtracting the two signals. Any deviation from zero in the difference of the two signals must be attributed to temporal noise so long as the non-destructive read process does not alter the quantity of charge in the pixel and that there is no additional charge generated between reads (the validity of this assumption is demonstrated in a later section). Event shot noise can not contribute to a deviation because the actual quantity of charge in any one pixel is exactly the same during both reads.

A more accurate estimation of temporal noise can be obtained by repeating the noise measurement on a single pixel many times and averaging the results. Alternatively, noise measurements may be conducted on a large number of pixels simultaneously and the results averaged. If temporal noise measurements are made on a subarray of "z" pixels and the computed differences between first and second reads exhibit the expected Gaussian

distribution, the mean difference for all measurements will approach zero as the number of measurements goes to infinity:

$$(14) \qquad \text{limit } z \dashrightarrow \infty \ \frac{1}{z} \sum_{i=1}^{i=z} (S_{(i,1)} - S_{(i,2)}) = 0$$

where:

$S_{(i,1)}$ = signal from pixel i, read 1

$S_{(i,2)}$ = signal from pixel i, read 2.

If z is sufficiently large to give good statistical results, the standard deviation from a zero mean caused by noise in the signal from one read, $\delta_{(N)}$ can easily be calculated for a group of pixels:

$$(15) \qquad \delta_{(N)} = \left(\frac{1}{2} \frac{1}{z-1} \sum_{i=1}^{i=z} (S_{i,1} - S_{i,2})^2\right)^{1/2}$$

and this is equal to the RMS read noise for a single non-destructive read (the 1/2 term in the above equation takes into account the fact that the read noise in both signals are equal and add in quadrature when the signals from the two reads are subtracted).

The principles discussed above were employed to measure the temporal read noise of the UA/CID-11B system. Noise measurements were conducted in the universal test chamber under the same conditions as those described in the section concerning gain measurements. The data used to determine read noise was collected from a 10 by 10 pixel subarray near the center of the

array. Results of repeated temporal read noise measurements on the UA/CID-11B system yield a figure of 0.84 +/-0.05 ADUs per read. This corresponds to 630 +/-40 electrons per read using the gain value calculated in the previous section.

One assumption that is made when measuring system gain is that the temporal read noise is independent of the quantity of charge in a pixel (see section on the mean-variance method). In order to determine if this assumption is correct, temporal read noise was measured at a variety of charge levels. The results of this experiment are plotted in Figure 2. It is evident from this data that read noise is independent of the quantity of charge in a pixel within the precision that the noise measurements allow.

TEMPORAL READ NOISE REDUCTION BY SIGNAL AVERAGING

As has been mentioned previously, a very significant advantage gained by the non-destructive read capability of the CID is the ability to reduce temporal read noise by averaging signals from a number of non-destructive reads. The effectiveness of signal averaging for noise reduction may be determined by a simple modification to the temporal noise measurement procedure discussed in the previous section. The modification involves the substitution of two sets of average signals computed from several non-destructive reads, $\bar{S}_{(i,1)}$ and $\bar{S}_{(i,2)}$, for the signals from two single non-destructive reads, $S_{(i,1)}$ and $S_{(i,2)}$ in Equation 15. If the temporal read noise consists of all frequencies (a "white" noise source) and the noise is uncorrelated from one read to the next, the effective temporal read noise of a mean signal will be equal to the square root of the number of averaged reads.

Figure 3 is a plot of the system read noise for a number of different values of averaged reads and the theoretical curve that would be followed if the read noise decreased exactly as the square root of the number of averaged reads. This plot shows a substantial reduction in effective temporal read noise as the number of averaged reads increases. By averaging only two reads, the effective temporal noise falls to 0.44 ADUs (326 electrons). By averaging 36 reads, the effective read noise falls to 0.21 ADUs (156 electrons). It is also evident from the plot that the observed reduction in noise does not exactly follow theory. This is to be expected since the bandwidth of the video amplifiers is limited and thus not all noise frequencies are averaged.

SOURCES AND MAGNITUDE OF FIXED PATTERN RESPONSE

A major source of fixed pattern response in CIDs can be attributed to variations in column electrode capacitance and the capacitance between row and column electrodes at each pixel site. For the UA/CID-11B system, there is an additional pattern response that arises from slightly different offsets in the two video amplifiers. These offsets are adjusted to a minimum, but small differences usually persist and are observed as different offsets for odd and even numbered pixels along a row.

The total fixed pattern response of the UA/CID-11B system was determined for a 100 pixel subarray near the center of the CID by first clearing the device of all charge, then reading the subarray multiple times and averaging the results. The RMS deviation from the mean signal was found to be 33 ADUs (24,500 electrons), which is a relative standard deviation of 1.5% of the linear operating range of the camera.

Since fixed pattern response is not a temporal noise source, it can be canceled out by measuring the offset of each pixel before an exposure is made, then digitally subtracting these offsets from the signals read from each pixel after the exposure. While this procedure completely eliminates fixed pattern response, any temporal read noise introduced from measuring pixel offsets will contribute to the total noise of a processed signal and thus multiple reads and signal averaging are employed to reduce the effective temporal read noise of the pixel offset measurements as much as possible.

PHOTOMETRIC RESPONSE FUNCTION

One basic requirement of a spectroscopic detector is that it exhibit a simple and well defined response to radiation. In the case of an array detector, an additional requirement is that the response of each detector element be resonably well matched. It is important to note, however, that while the response function of a detector should be simple, it is certainly not a requirement that the function be linear. Indeed, a different function such as a logarithmic response would often be at least equally suitable and in many cases preferable.

EXPECTED RESPONSE CHARACTERISTICS OF THE CID DETECTOR

If it is assumed that the quantity of charge in a pixel of the CID is a linear function of the sum of photons incident on that pixel, any deviations from linearity in the respose of the CID must be attributed to the charge quantization process. In a CID, determining the quantity of charge in a pixel is performed by transferring the charge from a collection and storage

capacitor to a charge sensing capacitor. When this charge transfer occurs, the change in potential of the sensing electrode can be expressed with the relation:

$$\Delta V = \frac{\Delta Q}{C} \tag{16}$$

where:

ΔV = change in potential on the column electrode

ΔQ = charge transferred

C = capacitance of the column capacitor.

This indicates that the CID detector should produce a signal which is a linear function of the quantity of charge in a pixel. Unfortunately, the capacitance of MOS capacitors typically change as a function of the potential across the capacitor which leads to a non-linear potential versus charge response (22). For this reason, a circuit known as a charge amplifier was chosen as the preamplifier on the UA/CID-11B system. This type of amplifier produces a output potential linearly proportional to the quantity of charge in a capacitor being sensed while maintaining a constant potential across the sensed capacitor.

MEAN RESPONSE FUNCTION OF THE UA/CID-11B SYSTEM

In order to investigate the photometric response characteristics of the UA/CID-11B system, a procedure was developed to measure the mean signal from a group of pixels as a function of the total number of photons striking the detector. In this experiment, the CID was first cleared of all charge, then the calibration LEDs of the universal test chamber were flashed on and off

to expose the CID to several highly reproducible bursts of photons. The signals from a 10 by 10 pixel subarray located near the center of the array were then read, averaged, and recorded. The expose and read process was continued until the device was saturated with charge and thus no longer responded to further exposure to light. The response function of the camera system was then determined by analyzing the mean signal versus exposure data.

Experimental equipment and conditions employed while conducting this evaluation were the same as those described in the section concerning system gain measurements. Also, the previously discussed technique of correcting for row-column crosstalk and amplifier offset was employed. To ensure the calibration LEDs would deliver reproducible quantities of light during each flash, heating of the LEDs (which would cause reduced output) was minimized by using a 40% on/off duty cycle and limiting the current during the "on" period to 15 milliamps. Also, the flash duration was timed with the camera controller to a precision of approximately 0.0001 millisecond.

A response function plot for the UA/CID-11B system is shown in Figure 4. It is apparent from this plot that the camera system has very linear response over a wide range, however, the plot does have a clearly non-linear "foot". Also present, but not as readily apparent is a non-linear "tail" to the plot. The foot of the plot can be attributed to the filling of charge traps in the silicon-silicon dioxide interface of the CID (22,23). Because of these traps, the first charge generated in a pixel is immobile and is thus unable to move from the charge collection capacitor to the charge sensing capacitor during the readout process. Charge traps are common to all surface channel MOS detectors such as the CID and surface channel CCDs (24). A technique commonly employed to avoid the non-linear operating

region in such detectors is to introduce a bias charge (or "fat zero") to fill the traps (19,24). Once all traps are filled, any further charge added to a pixel is completely mobile and thus gives a linear response function.

The tail of the response function plot occurs because pixels are beginning to reach their charge storage capacity. The roll off at the top end of the plot is gradual because the various pixels in the subarray have different charge capacities and sensitivities, thus they reach saturation at different times.

In order to observe the detailed behavior of the UA/CID-11B system in the linear operating region, a plot was made of the change in mean signal versus mean signal level (a pseudo first derivative plot) for the data in Figure 4. This is shown in Figure 5. It is apparent from this plot that the slope of the response function plot rises rapidly, then levels off at approximately 46 ADUs per exposure after 23 exposures. The slope then remains constant within 2.5 ADUs per exposure throughout 46 additional exposures. By translating exposure numbers to mean signal levels using the plot in Figure 4, it can be determined that the linear operating range of the CID-11B is from 900 ADUs (6.73×10^5 electrons) to 3100 ADUs (2.319×10^6 electrons), a range of 2200 ADUs (1.646×10^6 electrons). The deviation from linearity over this range is expressed as a ratio of the maximum deviation in slope (2.5 ADUs/exposure) over the linear range (2200 ADUs) which is a deviation of 0.11%.

In yet another experiment, the response function for a number of individual pixels was estimated in a manner nearly identical to the mean response function measurement. The same equipment was used for these measurements and the only difference in procedure was that instead of averaging the data from the pixels of a subarray, the data from each pixel

was individually recorded. Figure 6 consists of plots of typical data from five selected pixels of the subarray. Two important features are apparent in these plots, the first is that the response function of the individual pixels is very similar to the mean response function of the subarray. The second feature to note is that the slope of each plot is different. Since the conditions of the experiment are the same for each pixel and the calibration LEDs have been observed to illuminate the array uniformly, the variation in slope for these plots must be attributed to variations in sensitivity for these pixels.

CAUSES OF SENSITIVITY VARIATIONS

Probable causes of sensitivity variations in a CID are small deviations in row and column electrode widths and silicon dioxide layer thicknesses at each pixel site. This leads to differences in the capacitance of each column electrode, which in turn leads to sensitivity variations for pixels located on different columns. Also, these mechanical variations alter the size and magnitude of electric field penetration into the epitaxial layer, thereby changing the effective charge gathering area of a pixel. Variations in the thickness of the various oxide layers leads to variations in optical interference effects at any given wavelength, which implies that to some degree pixel sensitivity variations will be dependent upon the wavelength of incident light.

MAGNITUDE OF SENSITIVITY VARIATIONS

The relative sensitivities of each pixel of the 10 by 10 subarray discussed earlier were determined by the following experiment. First, the array was cleared of charge, then the calibration LEDs were used to put

enough charge in the pixels to bring the device into the linear operating range. The subarray was then read and the signal from each pixel in the subarray recorded. Next, the LEDs were again used to introduce charge into the pixels until the top end of the linear range was reached. The subarray was again read and the signal from each pixel recorded. The mean increase in signal for the pixels of the subarray was calculated to be 2193 ADUs and the standard deviation of the signals 115 ADUs. Event shot noise from the generation of charge contributes 45 ADUs to this figure, but the remainder (106 ADUs) must be attributed to sensitivity differences in the pixels. This is an approximately 5% relative standard deviation in pixel sensitivities.

SPECTRAL RESPONSE OF THE CID-11B

Charge injection devices constructed with processes and structures similar to the CID-11B have been shown to respond to radiation from the ultraviolet to near infrared wavelength range (14,25). The sensitivity of a CID at any wavelength is strongly affected by both the photo-optical properties of silicon and the electrodes and dioxide layers that overlay the silicon. The sensitivity of a CID typically falls in both the near infrared and ultraviolet wavelength regions but for different reasons. The diminished sensitivity in the near IR can be attributed to the decreasing absorbtion coefficient of silicon at longer wavelengths. As the absorbtion coefficient decreases, photons are either absorbed deep in the epitaxial layer or pass entirely through the epitaxy and are absorbed in the bulk silicon (at 900 nm, approximately 50% of all photons pass through the

epitaxy). The charge generated by photons absorbed deep in the epitaxy are more likely to undergo charge recombination before the charge can be collected at a pixel site. Charge generated in the bulk silicon can not be collected by a pixel because it can not cross the P-N junction of the bulk-epitaxy interface.

Decreased sensitivity for a CID in the ultraviolet wavelength region can be attributed to a variety of effects including increased reflection of photons from the surface of the CID due to the greatly increased index of refraction for silicon at shorter wavelengths. Another major effect responsible for lowering UV sensitivity of the CID is the absorbtion of photons by the polysilicon electrodes overlaying the epitaxial layer of the device (25).

Because the sensitivity of a detector at any given wavelength is a very important parameter when that detector is being considered for use in spectroscopic applications, the quantum yield (equivalent electrons collected per incident photon) of the CID-11B was measured as a function of wavelength. This measurement was made by determining the quantity of charge generated in a subarray of pixels during a known integration period due to photons from a monochromatic source of known flux and wavelength. In order to facilitate quantum yield measurements in the ultraviolet wavelength region, the glass window of the CID was removed and replaced with a quartz window. After quantum efficiency measurements were performed on this modified device, the quartz window was removed and a 200 A layer of coronene was sublimed onto the surface of the CID. The quartz window was then replaced and the measurements repeated. The coronene overcoat was applied in an attempt to improve the sensitivity of the CID-11B in the ultraviolet wavelength region. Coronene absorbs ultraviolet photons and fluoresces in

the blue-visible region where the CID is more sensitive. Therefore, if the absorbance and fluorescence yield is sufficiently high, there should be an overall increase in sensitivity for the device. Coronene overcoats have been successfully employed to improve the ultraviolet sensitivity of a charge coupled device (26).

QUANTUM YIELD MEASUREMENTS

The apparatus constructed to perform quantum yield measurements is diagrammed in Figure 7 and a list of equipment used appears in Table 1. In reference to Figure 7, the light source (A) is a dual tungsten/deuterium source. The tungsten source was used for measurements in the 400 nm to 900 nm range and the deuterium source was used from 200 nm to 400 nm. The monochromator (B) and wavelength drive (C) is used to select the desired wavelength. The output of the monochromator is directed into the input port of an integrating sphere (D), which creates a uniform photon flux at the exit port. Interference filters (E) were used when necessary to reduce stray light and second order wavelengths from the monochromator. A computer controlled electronic shutter (F) was used to control the integration times for the camera system. An LED inside the integrating sphere (G) was used to provide the bias flash to put the CID in a linear response region (see previous section).

The procedure employed for conducting quantum yield measurements was as follows. First, the photon flux at the output port of the integrating sphere was determined for a number of wavelengths. This was accomplished by measuring the photocurrent from a calibrated photodiode of known surface area (H) with a calibrated electrometer (I) located at a known distance from the sphere. The flux was determined at 25 nm increments from 200 nm to 400

nm and 50 nm increments from 400 nm to 900 nm. In order to have sufficient throughput for the flux determinations, it was necessary to open the entrance and exit slits of the monochromator to 0.2 cm in the 200 nm to 400 nm wavelength range, and 0.1 cm in the 400 nm to 900 nm range. The spectral bandpass was 4.0 nm and 2.0 nm, respectively.

To complete the quantum yield measurements, the photodiode was removed from the apparatus and the camera system attached such that the surface of the CID was the same distance from the exit port of the integrating sphere as the photodiode had been. The quantity of charge generated in a subarray of pixels during a known integration period was then determined at the same wavelengths that flux measurements were made. This was accomplished by first closing the electronic shutter at the input of the integrating sphere, then clearing the CID of all charge. The LED was then flashed until sufficient bias charge was created in the subarray to ensure a linear response function (see previous section). The mean signal due to the bias charge was then read and stored before the exposure to light from the integrating sphere was made (the signal was corrected for row-column crosstalk and amplifier offset in the same manner as previously discussed). The electronic shutter was opened for periods ranging from 1 to 300 seconds depending upon the wavelength used in the measurement. After the shutter was closed, the corrected mean signal from the subarray was read again. The two signals were then subtracted and multiplied by the system gain. This yields the quantity of charge generated during the integration period from which the mean rate of charge generation can be determined. By normalizing the charge generation rates from the CID and the photodiode and correcting for the quantum efficiency for the photodiode, the quantum yield of the CID was calculated.

Results of quantum yield measurements for the CID-11B are shown in Figure 8. Two lines are plotted from 200 nm to 400 nm, the upper line for the device after the coronene coating was applied and the lower for the uncoated device. From 400 nm to 900 nm the device exhibits no significant differences in quantum yield plots before and after the coating was applied, and therefore only one curve is plotted. The peak quantum yield recorded is 22.5% at 550 nm and it falls to 4% at 900 nm and 7% at 400 nm. There is a local minima in the curve at 350 nm for both coated and uncoated devices, but then the curves rise again reaching a local maxima at 275 nm. The CID-11B has a protective silicon dioxide overcoat of approximately 500 nm thickness (27). It is highly probable that this dielectric layer acts as an antireflection coating which would account for the maximum quantum yield at 550 nm and the high quantum yield at 275 nm. The coronene coating increased the quantum yield significantly in the 200 nm to 400 nm range. The greatest gain is at 200 nm where the uncoated device had no measureable response and the coated device has a 4% quantum yield.

SUMMARY

The CID appears to be uniquely qualified among imaging detectors to fulfill those requirements for an imaging spectroscopic detector presented at the beginning of this manuscript. The sensitivity of the CID-11B has been shown to be very good over a wide spectral range. The effective readout noise can be made to be very low, and the device is not susceptible to readout lag or blooming. In addition, this device has a highly linear response function and, when operated at cryogenic temperatures, exhibits

virtually no thermal charge generation. While the CID-11B does suffer from a form of spatial pixel crosstalk, this effect is both understood and easily compensated for.

One of the most outstanding features of a CID based detection system is the opportunity to synthetically increase the already high (10^4) dynamic range of the device through the use of variable integration times on select portions of the array. This capability is only possible through the CIDs unique destructive/non-destructive readout modes and pseudo random pixel access.

In conclusion, these characterization studies indicate that the CID is capable of excellent performance as a general purpose spectroscopic detector. While novel and highly specialized electronic equipment and data manipulation algorithms are required to employ the CID for spectroscopic measurements, there are no limitations on the applicability of a CID detection system in a modern laboratory.

ACKNOWLEDGMENT

This research was partially supported by the Office of Naval Research.

REFERENCES

1. Stubley, E.A.; Horlick, G. Appl. Spectrosc. 39, 5 (1985) 805.

2. Talmi, Y. Anal. Chem. 47, 7 (1975) 268A.

3. Talmi, Y. Anal. Chem. 45, 7 (1975) 658A.

4. Busch, K.W.; Malloy, B. ACS Symposia Series No. 102 (1979), p.27.

5. Talmi, Y.; Simpson, R.W. Appl. Opt. 19 (1980) 1401.

6. Horlick, G. Appl. Spec. 30 (1976) 113.

7. RCA S10504 Technical Bulletin.

8. Texas Instruments TI4849 Technical Bulletin.

9. Tektronics CCD Imager Technical Bulletin.

10. Michon, G.J.; Burke, H.K. IEEE Digest of Technical Papers (1973), p.138.

11. Michon, G.J.; Burke, H.K. IEEE International Solid State Circuits Conf. (1974), p. 26.

12. Michon, G.J.; Burke, H.K.; Brown, P.M. Proceedings of Symposium on Charge-Coupled Device Technology for Scientific Imaging Applications, Sponsored by the Jet Propulsion Laboratory (March 6-7, 1975), pp.106-115.

13. Sachs, Fred A. Electro-Optical Systems Design (October 1975), 34.

14. Lewis, H.; Denton, M.B. J. Automatic Chem. 3 (1981), 9.

15. Denton, M.B.; Lewis, H.A.; Sims, G.R. ACS Symposium Series No. 236 (1983), p. 133.

16. Michon, G.J.; Burke, H.K.; Vogelsong, T.L.; Wang, K. SPIE Proceedings 203 (1979) 66.

17. Sims, G.R.; Denton, M.B. ACS Symposium Series No. 236 (1983), p. 117.

18. Mortara, L.; Fowler, A. SPIE Proceedings 290 (1981), 28.

19. Aikens, R.S.; AURA Engineering Technical Report No. 66 (1980).

20. Dereniak, E.L.; Crowe, D.G. Optical Radiation Detectors. Wiley, New York (1984) p. 237.

21. Aikens, R.S.; Lynds, C.R.; Nelson, R.L. SPIE Proceedings 78 (1976), 65.

22. D.A. Fraser, The Physics of Semiconductor Devices, Oxford University Press (1983) p. 118.

23. Lamb, D.R. Thin Solid Films 5 (1970) 247-276.

References cont.

24. Tompsett, M.F. J. Vac. Sci. Technol. 9 (1972) 1166-1181.

25. Brown, D.M.; Gheggo, M; Garfinkel, M. IEEE International Solid State Circuits Conf. (1975).

26. Blouke, M.M.; Cowens, M.W.; Hall, J.E.; Westphal, J.A.; Christensen, A.B. Applied Optics 19, No. 19 (1980), 3318.

27. Carbone, J. General Electric Co., personal communication (1985).

TABLE 1

EQUIPMENT USED IN QUANTUM YIELD MEASUREMENT APPARATUS

MONOCHROMATOR:	model EU-700 scanning monochromator grating: 1180 l/mm, 250 nm blaze (GCA/McPhearson Acton, Mass.)
LIGHT SOURCE:	model EU-701-50 dual tungsten/deuterium light source (Heath Benton Harbor Mich.)
PHOTODIODE:	model UV-444BQ calibrated silicon photodiode (EG+G Electro-Optics division Salem, Mass.)
ELECTROMETER:	model 110 laboratory photometer (Pacific Precision Instruments Concord, Calif.)
INTEGRATING SPHERE:	surplus 4 inch integrating sphere coated in these laboratories with Eastman White Reflectance Paint #6080.

CHARACTERIZATION OF A CHARGE INJECTION DEVICE CAMERA SYSTEM FOR SPECTROCHEMICAL MEASUREMENTS

Figure Captions

Figure 1: Mean-variance plot of the UA/CID-11B camera system. See text for explanation.

Figure 2: System read noise as a function of mean signal level. This confirms system read noise is independent of pixel charge content.

Figure 3: Reduction in effective system read noise as a function of number of averaged reads. Upper curve is from experimental data; lower curve is theoretical.

Figure 4: Mean photometric response curve demonstrating the linearity of the UA/CID-11B camera system.

Figure 5: Pseudo first derivative plot of the photometric response curve from which the range of linear behavior is determined.

Figure 6: Response function plot of eight individual pixels. These plots show that individual pixels have linear response functions despite the different sensitivities.

Figure 7: Block diagram of apparatus used to determine spectral response of the CID-11B. See text for explanation.

Figure 8: Spectral response curves for coronene coated and uncoated CID-11B sensors.

Figure 1

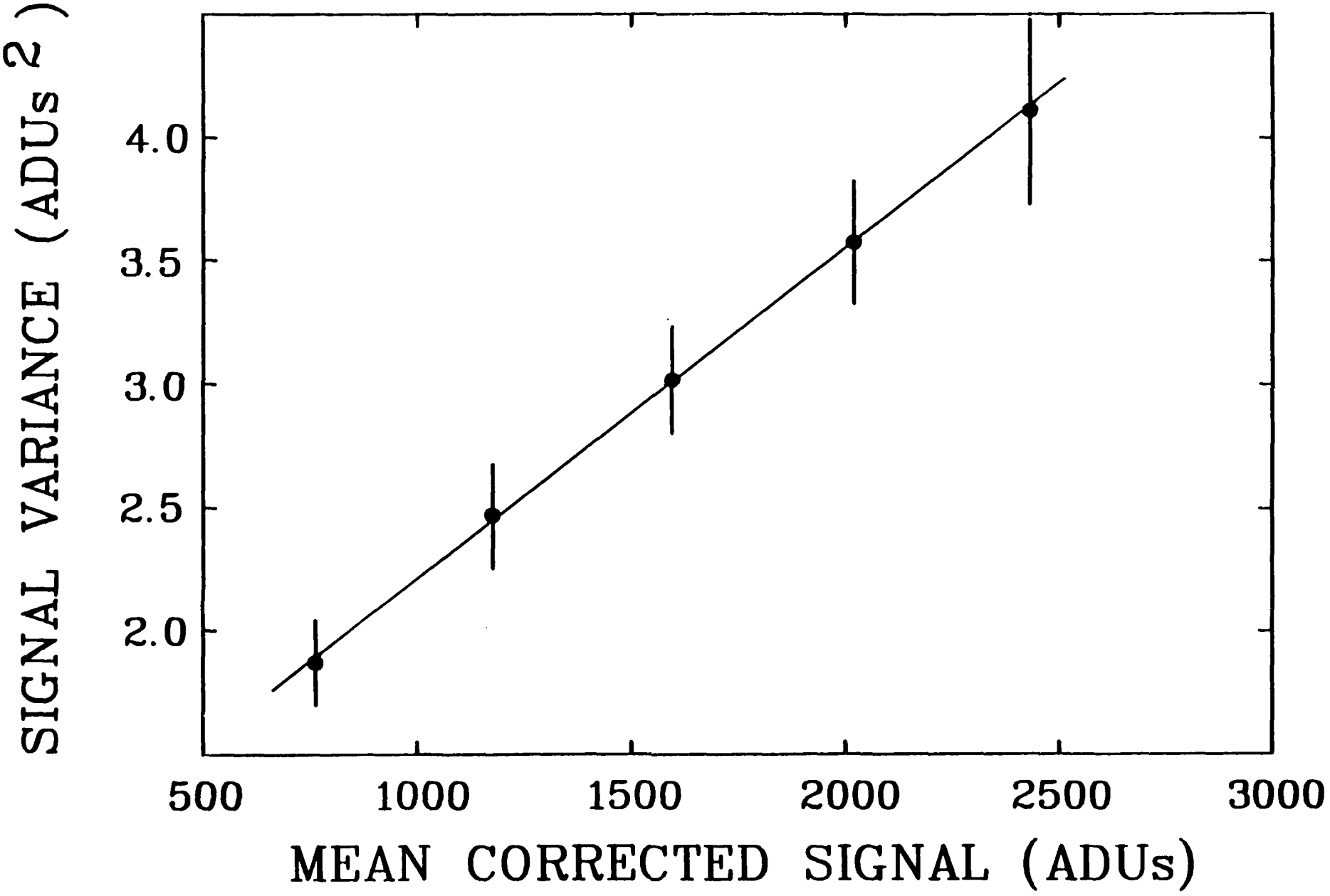
SIGNAL VARIANCE (ADUs 2)
4.0
3.5
3.0
2.5
2.0
500
1000
1500
2000
2500
3000
MEAN CORRECTED SIGNAL (ADUs)

Figure 2

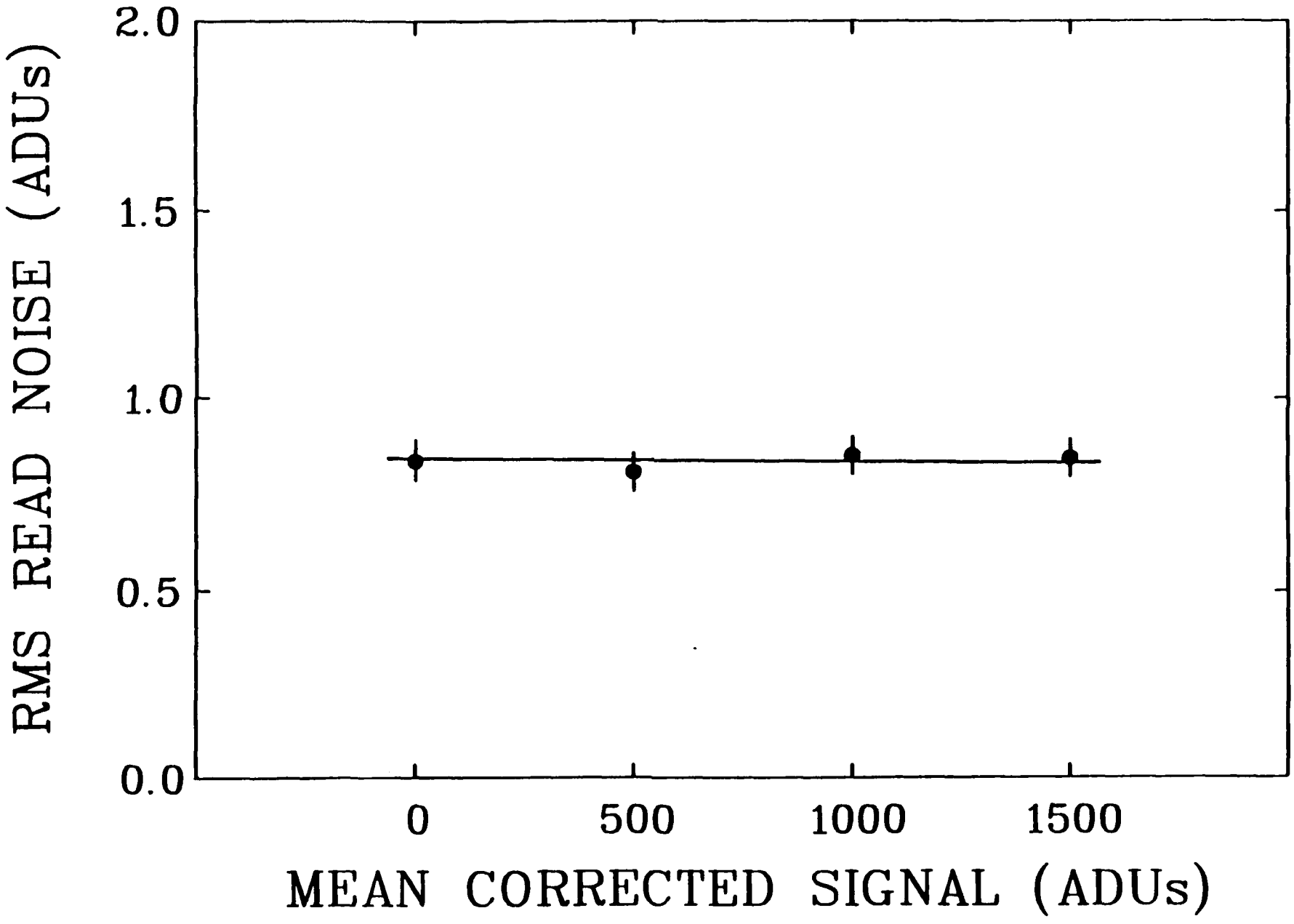
RMS READ NOISE (ADUs)
2.0
1.5
1.0
0.5
0.0
0
500
1000
1500
MEAN CORRECTED SIGNAL (ADUs)

Figure 3

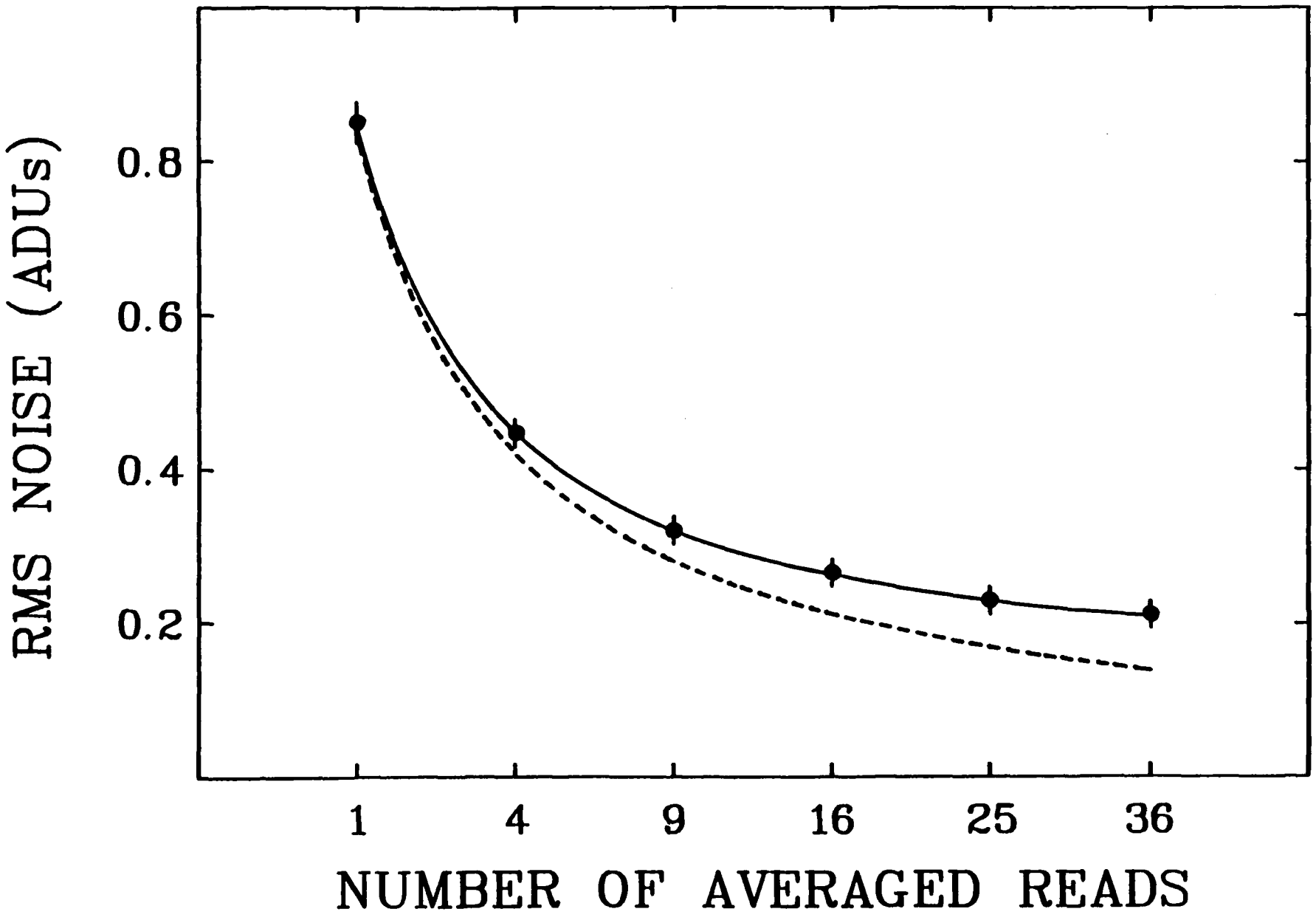
RMS NOISE (ADUs)
0.8
0.6
0.4
0.2
1
4
9
16
25
36
NUMBER OF AVERAGED READS

Figure 4

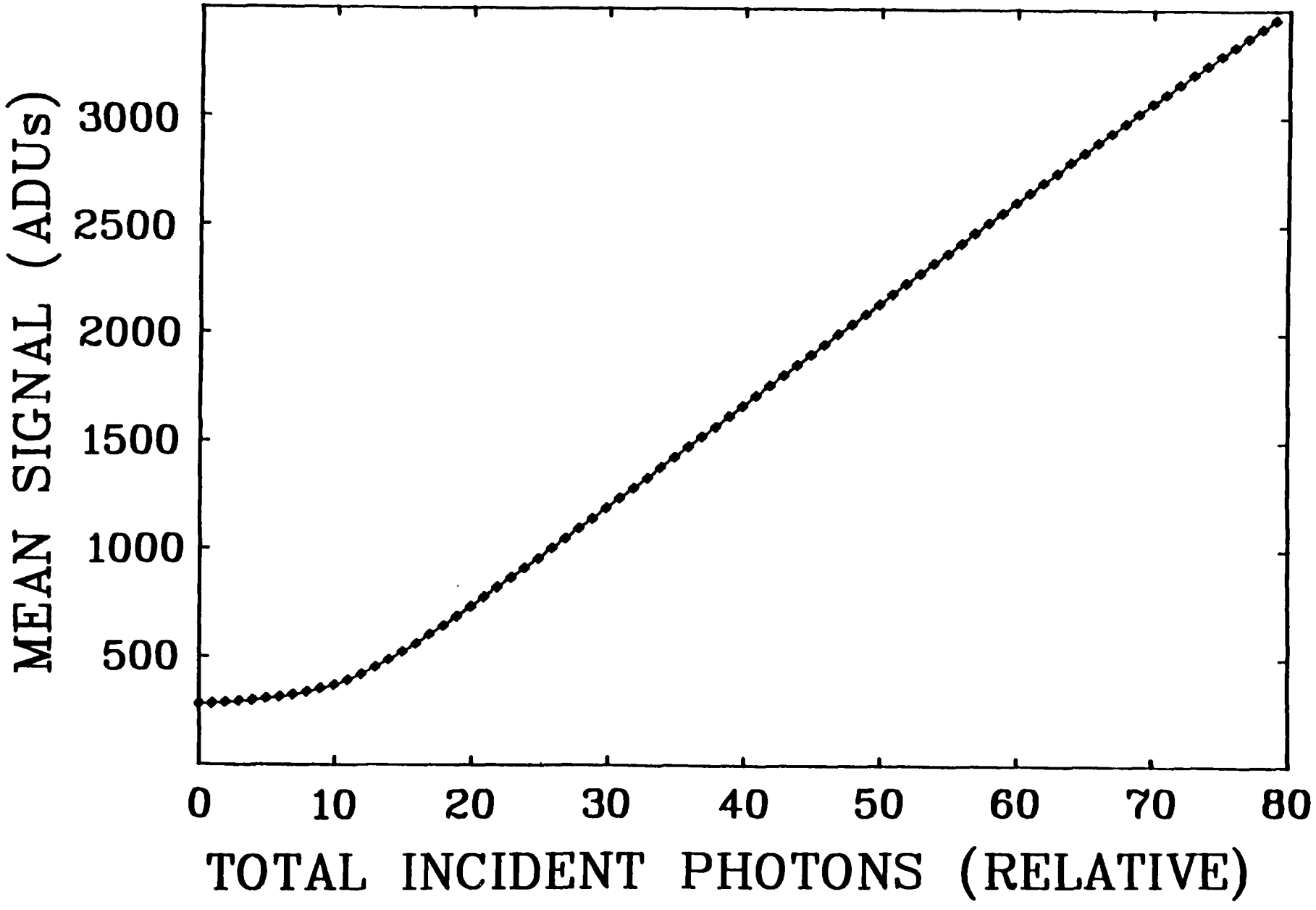
MEAN SIGNAL (ADUs)
3000
2500
2000
1500
1000
500
0
10
20
30
40
50
60
70
80
TOTAL INCIDENT PHOTONS (RELATIVE)

Figure 5

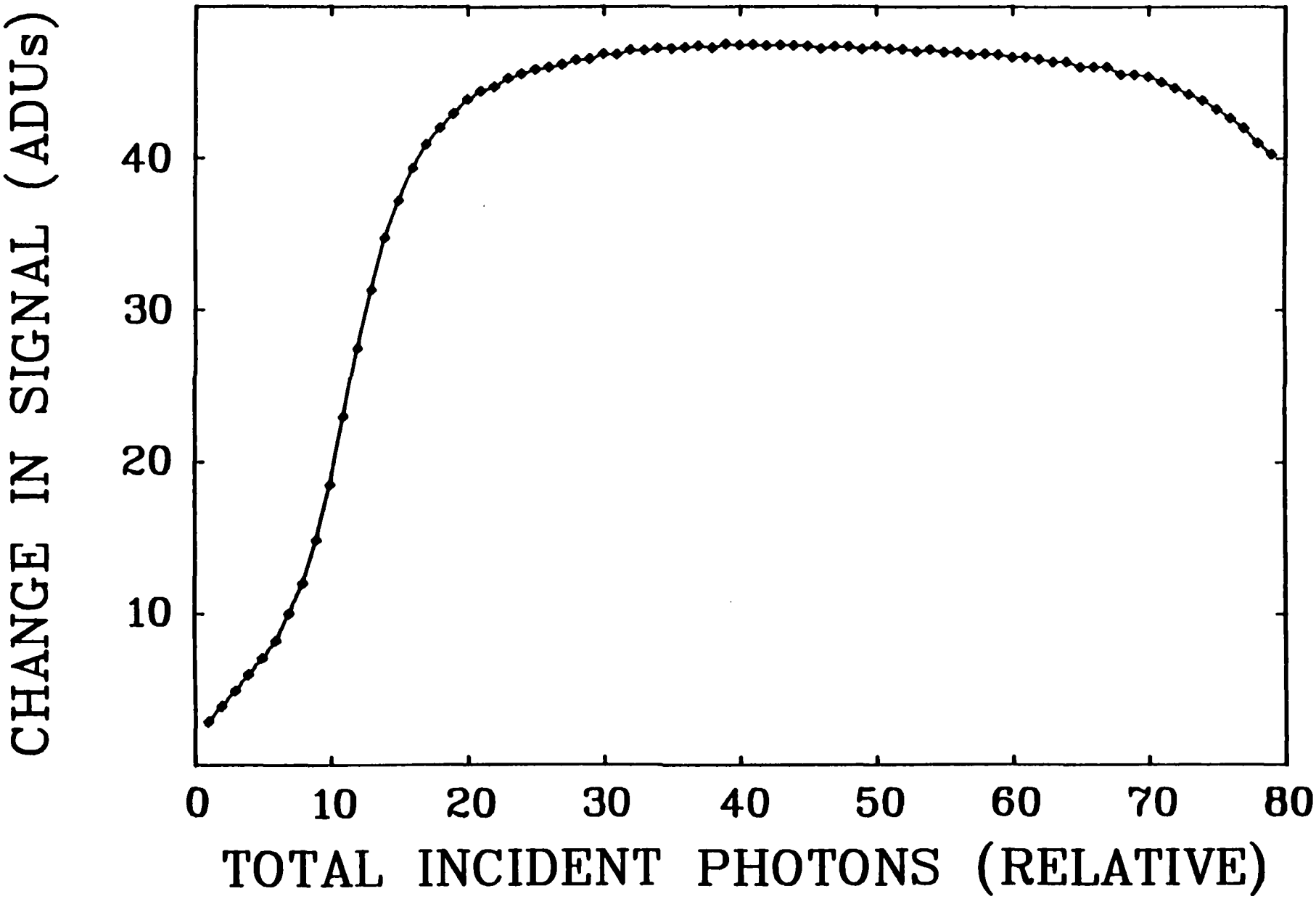
CHANGE IN SIGNAL (ADUs)
10
20
30
40
0
10
20
30
40
50
60
70
80
TOTAL INCIDENT PHOTONS (RELATIVE)

Figure 6

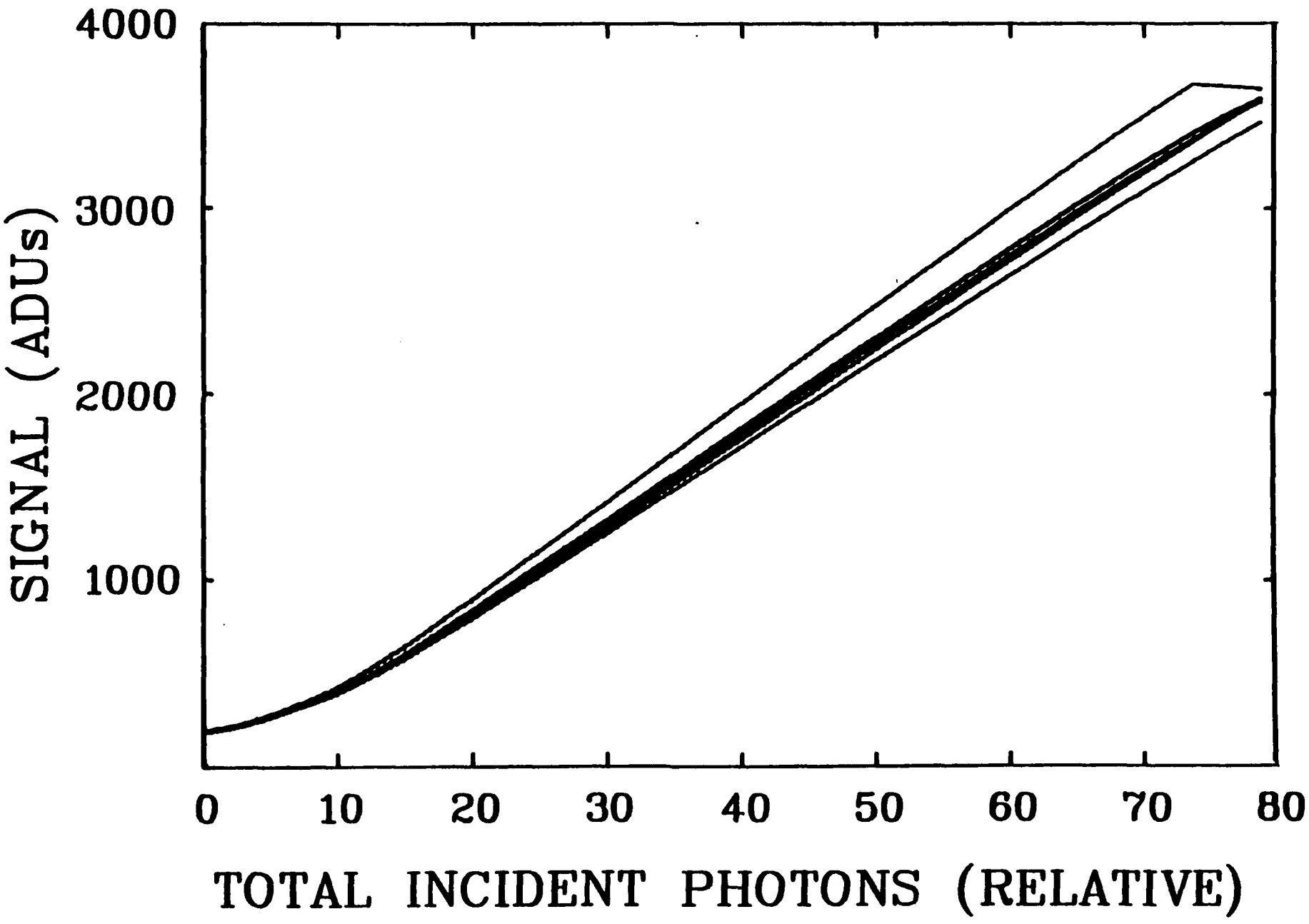
4000
3000
2000
1000
SIGNAL (ADUs)
0
10
20
30
40
50
60
70
80
TOTAL INCIDENT PHOTONS (RELATIVE)

Figure 7

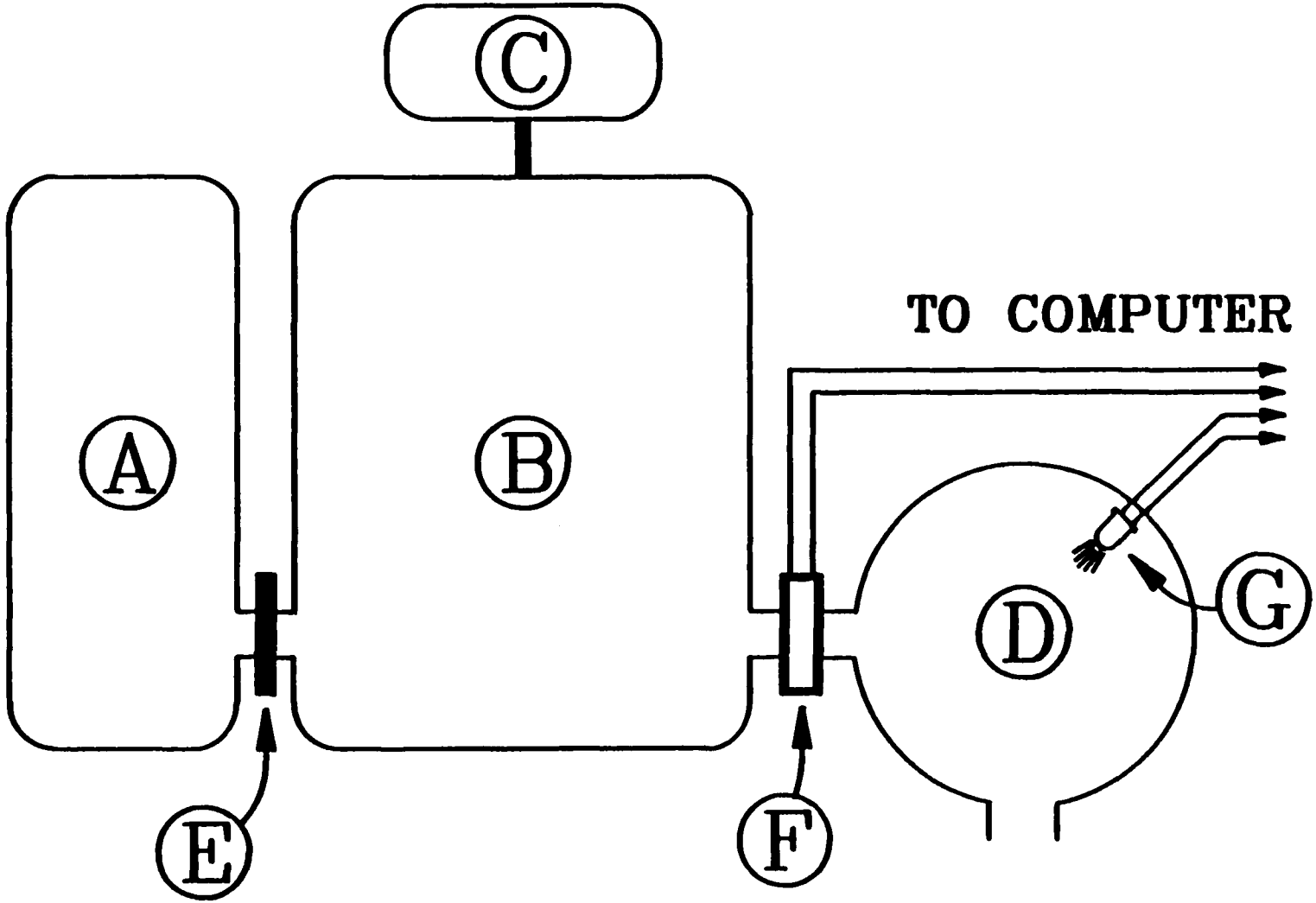

Figure 8

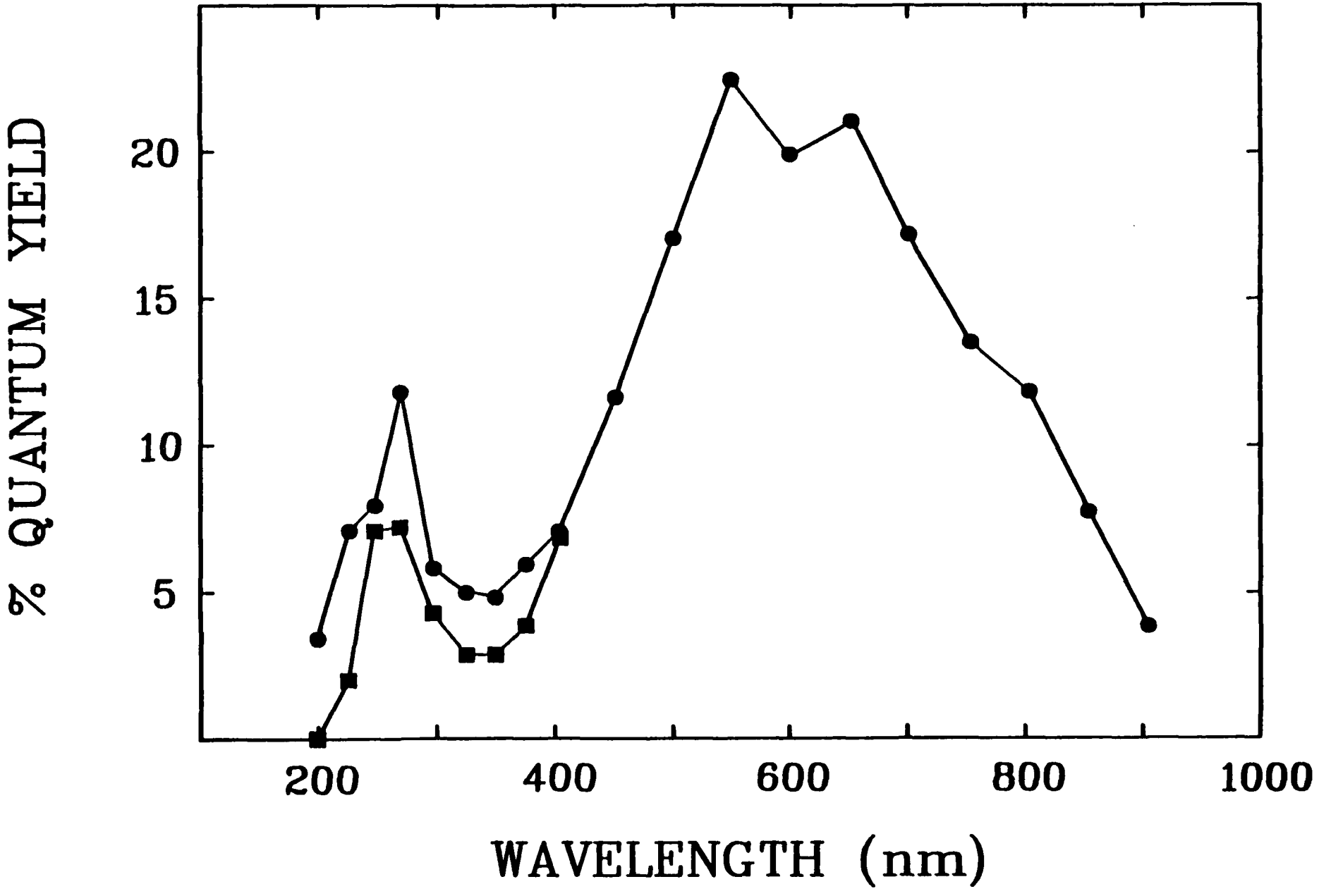

END

FILMED

2-86

DTIC